Chinese Chemical Letters 36 (2025) 110017

Contents lists available at ScienceDirect

Chinese Chemical Letters

journal homepage: www.elsevier.com/locate/cclet

Cyclodextrin-boosted photocatalytic oxidation for efficient bisphenol A removal

Qinwei Lu[a], Jinjie Lu[a], Juying Lei[a,b], Xubiao Luo[c], Yanbo Zhou[a,c,*]

[a] State Environmental Protection Key Laboratory of Environmental Risk Assessment and Control on Chemical Process, East China University of Science and Technology, Shanghai 200237, China
[b] Shanghai Institute of Pollution Control and Ecological Security, Shanghai 200092, China
[c] School of Life Science, Jinggangshan University, Ji'an 343009, China

ARTICLE INFO

Article history:
Received 22 February 2024
Revised 7 May 2024
Accepted 15 May 2024
Available online 16 May 2024

Keywords:
Photocatalysis
β-Cyclodextrin
Bisphenol A
Confined catalysis
Organic free radical

ABSTRACT

Wastewater contains various high-risk trace organic pollutants, such as antibiotics and endocrine disruptors, which seriously restrict wastewater reuse. Cyclodextrin-based functional materials show great potential in the removal of trace pollutants because of their adsorption catalytic synergy. Clarifying the synergistic mechanism of cyclodextrin in oxidation is the key issue in confined catalytic oxidation process design. In this work, we fabricated a $BiOIO_3$@BiOBr/β-CD heterojunction photocatalyst to study the synergistic mechanism of cyclodextrin in the photocatalytic oxidation process. The synergistic mechanism of cyclodextrin was investigated by combining radical chemistry, electrochemistry, spectroscopy, and time-dependent density functional theory. Results showed that the excited intermediate free radicals played an important role in promoting the photocatalytic degradation process. The heterojunction photocatalyst loaded with β-cyclodextrin (β-CD) at the electronic end ($C_{[Cat.]} = 0.2$ mg/mL) removed about 97% of bisphenol A (BPA) within 30 min, and the first-order kinetic constant ($k_{CDBIB} = 0.112$ min^{-1}) was about twice that of the unloaded β-CD ($k_{BIB} = 0.057$ min^{-1}). Cyclodextrin loading improved the photocatalytic performance of the heterojunction and stimulated the intermediate to increase the free radical yield and regulate the reaction path.

Human activities have caused large-scale water pollution, which has further exacerbated the crisis of water scarcity [1]. The regeneration and reuse of urban sewage are increasingly attracting widespread attention [2]. Before the regeneration and reuse of urban sewage, the pollutants contained in it must be effectively removed to eliminate negative effects on human health, the natural environment, and other aspects [3]. Endocrine pollutants represented by bisphenol A have attracted widespread attention due to their biological toxicity and widespread presence [4].

Among various advanced treatment technologies, photocatalytic technology with free radical oxidation as the core has obvious advantages [5]. However, the photocatalytic oxidation process has the disadvantages of low degradation rate and no selectivity for the degradation of pollutants, which cannot meet the requirements of efficient, low-carbon removal of micropollutants in water [6].

Cyclodextrin has the characteristics of internal hydrophobicity, external hydrophilicity, modifiable hydroxyl group, and high charge density [7]. Previous studies have shown that catalysts based on β-cyclodextrin (β-CD) show good catalytic oxidation performance for phenolic pollutants due to their role in accelerating photoelectron transport [8]. They exhibit excellent performance in removing BPA and can replace precious metals, such as gold, as catalysts during the oxidation process [9]. However, in a β-CD-based catalytic oxidation system, the intermediate products (such as phenol) have high concentrations, but no catalyst poisoning phenomenon occurs to inhibit the reaction [9]. Therefore, the accelerated degradation mechanism of cyclodextrin for phenolic pollutants cannot be the enrichment of pollutants and the acceleration of photoelectron transport. This unclear efficiency enhancement mechanism has limited the development of carbon-based catalysts and their application in urban sewage treatment. Therefore, we speculate that β-CD could also make pollutants and their degradation products play the role of electron donors in addition to enhancing catalyst performance [10]. Similarly, cucurbit[7]uril can reduce perylene diimide derivatives to supermolecule perylene diamine radical anions under light conditions [33]. Bismuth oxyiodide($BiOIO_3$),

* Corresponding author at: State Environmental Protection Key Laboratory of Environmental Risk Assessment and Control on Chemical Process, East China University of Science and Technology, Shanghai 200237, China.
E-mail address: zhouyanbo@ecust.edu.cn (Y. Zhou).

https://doi.org/10.1016/j.cclet.2024.110017
1001-8417/

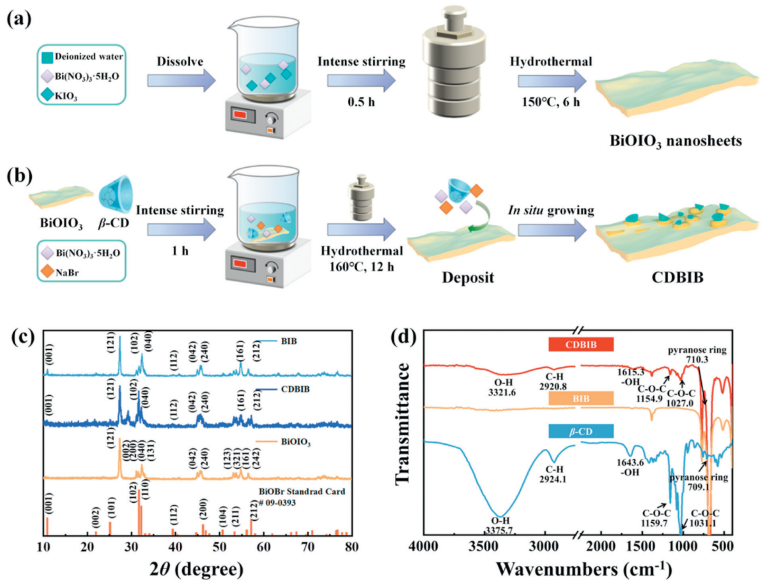

Fig. 1. Schematic of the fabrication of (a) $BiOIO_3$ nanosheets and (b) $BiOIO_3$@BiOBr modified with β-CD. (c) XRD patterns and (d) FT-IR spectra of BIB, CDBIB, and β-CD.

as an asymmetric semiconductor material, exhibits high efficiency in charge transfer and carrier separation. BiOBr is usually used to form heterojunctions with $BiOIO_3$ due to its suitable valence band and conduction band positions and visible light absorption capacity.

In this work, a $BiOIO_3$@BiOBr heterojunction photocatalyst was used as a model catalyst to verify the abovementioned speculation. The photocatalyst was fabricated by a simple two-step hydrothermal method, and β-CD was loaded on the electronic end of the heterojunction, and the structure of heterojunctions can better determine the direction of electron flow with β-CD (Figs. 1a and b). The photocatalytic oxidation and β-CD synergistic mechanisms were discussed. The possible excitation effect of cyclodextrin on intermediate products was studied by spectroscopy, free radical chemistry, and theoretical calculation.

The physical structure and surface chemistry of CDBIB were characterized by X-ray diffraction (XRD) and Fourier transform infrared (FT-IR) spectra. Fig. 1c presents the XRD patterns of BIB and CDBIB. The distinct peaks of BIB and CDBIB at 2θ values of 27.4°, 32.4°, 45.7°, and 54.8° matched the (121), (040), (240), and (161) crystallographic planes of $BiOIO_3$ (ICSD #262019), respectively [11]. Meanwhile, the diffraction peaks at 2θ values of 10.9°, 31.7°, and 57.1° matched the (001), (102), and (212) planes corresponding to BiOBr (JCPDS #09–0393), respectively [12]. These results indicate that $BiOIO_3$ and BiOBr successfuly combined in BIB and CDBIB. The FTIR spectra of BIB and CDBIB are presented in Fig. 1d. The peaks at 332.16, 292.08, and 1154.9 cm^{-1} belonged to O–H and C–H stretching vibrations and C–O bending vibration, respectively. The peak at 710.3 cm^{-1} was attributed to the pyranose ring vibration of β-CD and indicated the inclusion of β-CD in the composite catalyst [13]. Notably, the peak detected in CDBIB red-shifted compared with the standard characteristic peak of β-CD, which demonstrates that β-CD interacted with BIB rather than being simply mixed physically [14].

The SEM and TEM images of BIB and CDBIB are shown in Figs. 2a–f. BIB exhibited nanosheet morphology with in-situ grown BiOBr nanoparticles. This morphology directly indicates the heterojunction structure of BIB. After loading cyclodextrin, the stacking morphology of CDBIB did not change considerably. However, the BiOBr particles on the surface of the $BiOIO_3$ nanosheets were fine and may have enhanced the adsorption and catalytic abilities. The TEM images showed that the lattices between $BiOIO_3$ and BiOBr

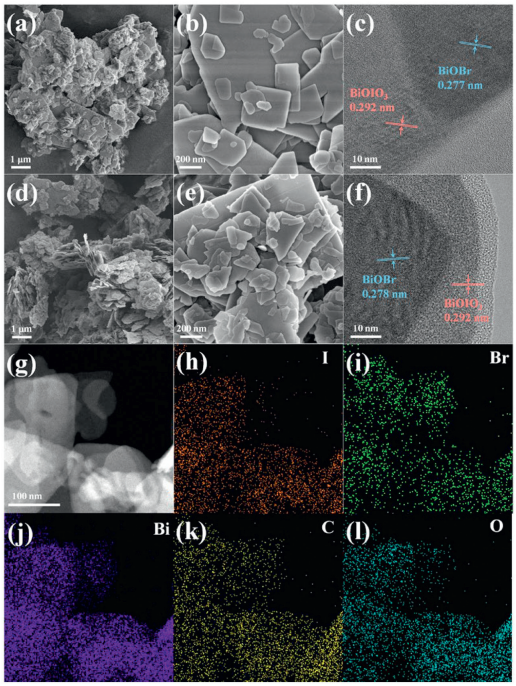

Fig. 2. (a) SEM and (b, c) TEM images of BIB. (d) SEM image of CDBIB. (e, f) TEM and (g–l) mapping images of CDBIB.

were staggered (BiOBr 0.277 nm [13], $BiOIO_3$ 0.292 nm [11]), and a layer of organic matter was attached to the surface. This result was proven by the elemental mapping of CDBIB (Figs. 2g–l and Fig. S1 in Supporting information).

The elemental states of the CDBIB were characterized by XPS (Fig. 3). The survey spectrum (Fig. 3a) indicated that Bi, I, Br, C, and O coexisted in CDBIB. The deconvolution of the C 1s peak of CDBIB (Fig. 3b) produced five peaks, and the peaks at 288.78, 286.15, and 284.58 eV were assigned to C=O–C, C–O, and C–C, respectively [15]. The peaks at 292.46 and 294.31 eV were ascribed to the C 1s in the carbonate and ester positions, which proved that β-CD was loaded on the surface of the catalyst rather than being simply mixed physically [16]. The O 1s spectra of CDBIB (Fig. 3c) showed peaks at

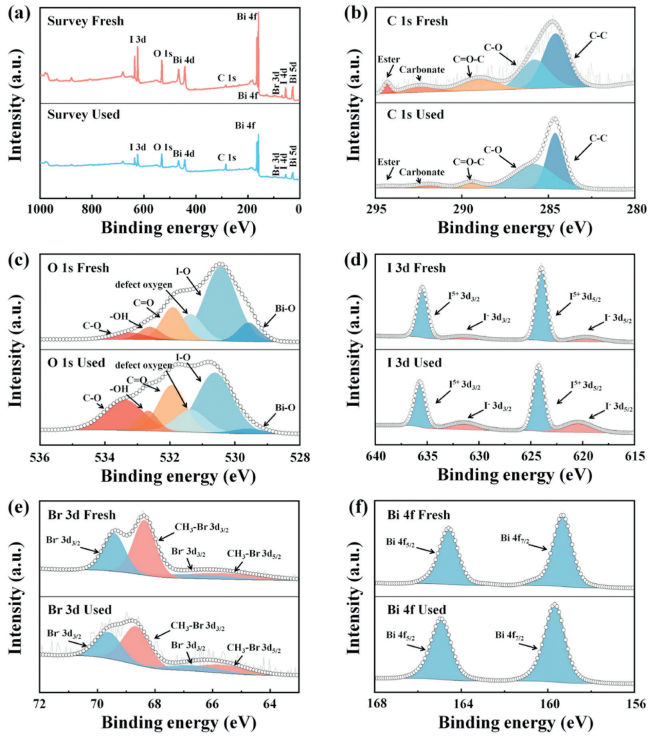

Fig. 3. (a) Survey XPS spectra of CDBIB before and after catalytic reactions. High-resolution XPS spectra of (b) C 1s, (c) O 1s, (d) I 3d, (e) Br 3d, and (f) Bi 4f.

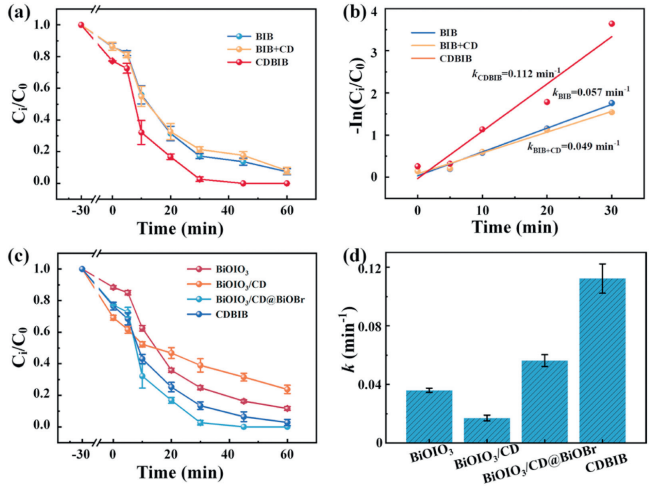

Fig. 4. (a) Removal efficiency of BPA by different catalysts and (b) corresponding degradation kinetics. (c) Removal efficiency of BPA by different β-CD loading methods and (d) corresponding degradation kinetics. Conditions: [Cat.] = 0.2 g/L, [BPA] = 10 mg/L, and $T = 20 \pm 1$ °C.

530.43 and 529.57 eV related to I–O and Bi–O, respectively. Another peak at 531.35 eV corresponded to oxygen vacancies on the heterojunction surface. The binding energy corresponding to the peaks of Br 3d at 68.36 and 68.41 eV was attributed to CH_3-Br $3d_{3/2}$ and $3d_{5/2}$, respectively, and revealed that β-CD was compounded on BiOBr. The FT-IR and XPS results proved that β-CD was loaded on the surface of the catalyst by a covalent bond. In addition, the little change of I 3d, Br 3d and Bi 4f deconvolution peaks proved the excellent cycling ability of the catalyst (Figs. 3d–f).

The photocatalytic oxidation effectiveness of CDBIB was evaluated using BPA as the target pollutant. Figs. 4a and b show the adsorption and photocatalytic degradation of BPA with different catalysts. CDBIB had a larger adsorption ability for BPA compared with

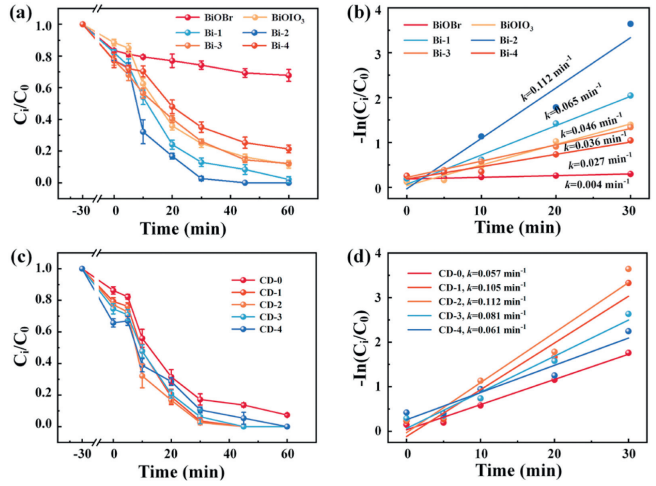

Fig. 5. (a) Catalytic activity of the catalysts with different BiOBr loading amounts and (b) the corresponding degradation kinetics. (c) Catalytic activity of the catalysts with different β-CD loading amounts and (d) the corresponding degradation kinetics.

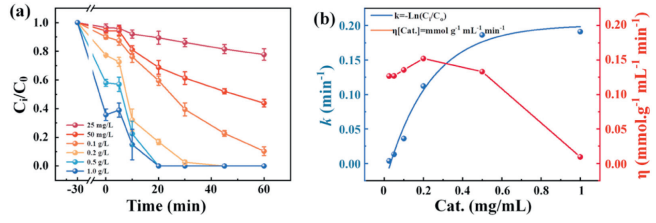

Fig. 6. (a) Removal efficiency of BPA for different catalyst dosages and (b) the corresponding degradation kinetics and catalyst utilization.

BIB due to the increased specific surface area and the provision of abundant adsorption sites by β-CD [17]. The CDBIB photocatalytic system removed about 97% of BPA within 30 min, closely aligning with the pseudo first-order dynamic model. The reaction kinetic constant of CDBIB ($k_{CDBIB} = 0.112$ min^{-1}) for BPA was about twice that of BIB ($k_{BIB} = 0.057$ min^{-1}). Notably, simple physical mixing did not improve the photocatalytic efficiency of the catalyst. However, the reaction rate decreased, possibly due to the competition of β-CD monomers for some ROS [18]. In addition, the loading of β-CD on the surface of $BiOIO_3$ or the holes of BIB cannot effectively enhance the photocatalytic oxidation ability of the catalyst (Figs. 4c and d). This conclusion is consistent with our speculation that β-CD capture negatively charged pollutants (phenolic pollutants) as electron donors to accelerate the catalytic oxidation process.

As the BiOBr loading increased, the photocatalytic activity of CDBIB initially increased and then decreased (Fig. 5a). The degradation rate constant (k) was 0.112 min^{-1} for Bi-2, 0.004 min^{-1} for BiOBr, and 0.046 min^{-1} for $BiOIO_3$ (Fig. 5b). The loading of BiOBr greatly enhanced the photocatalytic activity, which proved the formation of the heterojunction [19]. However, an excess of BiOBr particles was detrimental to photocatalysis because of the recombination of photo-generated electrons and holes [20]. In Fig. 5c, the adsorption of BPA increased with β-CD content, and the photocatalytic degradation rate was similar to the previous findings (Fig. 5d). The increase in the degradation rate was attributed to the enrichment of pollutants, and the decrease was due to excessive β-CD competing for ROS and covering the reaction sites [21]. The catalyst with the optimal loading ratio was named CDBIB for subsequent experiments.

Figs. 6a and b show the effect of catalyst amount on BPA degradation in the CDBIB systems and pseudo first-order rate constants,

Table 1
Comparison of degradation performance of photocatalytic oxidation system.

Catalyst	Conditions (mg/mL)	Pollutions (mg/L)	Kinetic (k, min^{-1})	Ref.
SH-CD-Au@CdS@MnO_x	1	BPA (20)	0.0904	[9]
CDP-TiO_2	0.5	BPA (20)	0.025	[21]
ACD-GO-TiO_2	1	NC (60)	0.040	[34]
CoS_x@BiOBr	0.4	CBZ (20)	0.024	[20]
$BiOIO_3$/g-C_3N_4	1	2,4,6-TCP (2)	0.016	[28]
2D/2D BiOBr/g-C_3N_4	1	BPA (20)	0.064	[44]
CDBIB	0.2	BPA (10)	0.112	This work

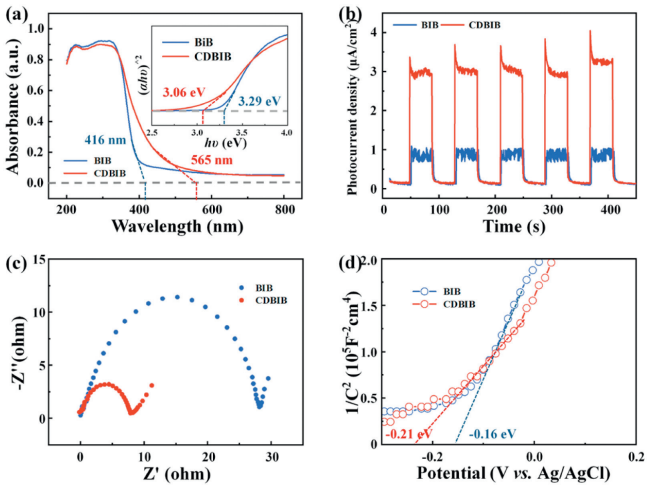

Fig. 7. (a) UV–vis DRS spectra and (insert) transformed Kubelka–Munk function against the photon energy plot of BIB and CDBIB. (b) Transient photocurrent responses of BIB and CDBIB (under 300 W of irradiation by a Xe lamp). (c) EIS Nyquist plots of different samples with the absence of light. (d) Mott–Schottky curve of BIB and CDBIB.

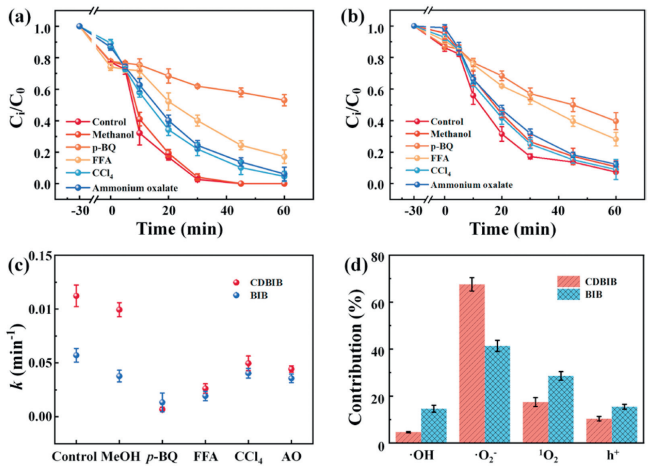

Fig. 8. (a) CDBIB photooxidation with different sacrificial agents, (b) BIB photooxidation with different sacrificial agents, (c) corresponding apparent rate (K_a) by CDBIB and BIB with different quenchers, and (d) contribution rate of oxidative species. Conditions: [Cat.] = 0.2 g/L, [BPA] = 10 mg/L, and [quencher] = 5 mmol/L.

respectively. With the increase in the catalyst amount, the reaction kinetic constant increased. The growth rate of the reaction kinetics decreased considerably when the catalyst amount reached 0.2 mg/mL. Catalyst utilization efficiency was applied (Eq. 1) to further evaluate the photocatalytic activity of CDBIB under different dosages [22]. Catalyst utilization efficiency represents the molar amount of pollutants that are photocatalytically oxidized per unit catalyst in unit time. Similar to the kinetic fitting results, 0.2 mg/mL CDBIB had the highest catalyst utilization rate and was used for the subsequent experiments.

$$\eta = \frac{\Delta \text{pollution}}{C[Cat.]}k \quad (1)$$

To compare the photocatalytic oxidation ability of CDBIB in this work with previous reports, Table 1 lists the photocatalytic oxidation rates of pollutants by different cyclodextrin based catalysts and bismuth based catalysts. The results indicate that the catalytic oxidation ability of CDBIB is much higher than that of common photocatalysts, and lower catalyst concentration is required during operation.

The photoelectrochemical properties were tested to effectively illustrate the accelerated electronic transmission ability and enhanced charge hole separation efficiency of CDBIB. From the UV visible diffuse reflectance (UV–vis DRS) spectra of the preprepared catalysts (Fig. 7a), the absorption boundary of BIB was determined at 416 nm, which could absorb limited visible light. The transformed Kubelka–Munk function showed that the band gap energies of BIB and CDBIB were 3.26 and 3.06 eV, respectively. The loading of β-CD greatly increased the absorption boundary of CDBIB (565 nm) and narrowed the band gap because of the localized surface plasmon resonance (LSPR) and electron polarization effects mediated by β-CD [23]. The decoration of β-CD led to a high photocurrent density (Fig. 7b) because of the polarization of the catalyst charge and the directional migration of electrons by β-CD [24]. Compared with the EIS Nyquist plot of BIB, the EIS Nyquist plot of CDBIB had a smaller Nyquist arc radius (Fig. 7c), indicating that CDBIB had lower resistance and faster electron migration than BIB. The calculation of the intercept of the Mott–Schottky curve (Fig. 7d) showed that the flat-band potentials of CDBIB and BIB were −0.21 and −0.16 eV, respectively. Given that the conduction band is usually 0.1–0.3 eV more negative than the flat-band potential, the conduction band of the catalyst was still lower than the oxygen reduction potential for generating superoxide radicals [25]. The experiments on photoelectrochemical properties further verified the promoting effect of β-CD on photocatalytic activity.

Scavenging tests were conducted on BIB and CDBIB to further elucidate the improvements in the photocatalytic ability of the heterojunction and the changes in the electron transport path by β-CD. As exhibited in Fig. 8a, p-benzoquinone (p-BQ) resulted in a dramatic decrease in the photocatalytic degradation of BPA, revealing the main role of $^{\bullet}O_2^-$. The loading of β-CD considerably increased the contribution of superoxide to the oxidative degradation of BPA (Figs. 8b and c), and the main ROS in the BIB system were singlet oxygen and superoxide (Fig. 8d). This result can be ascribed to the fact that β-CD loaded on BiOBr captures pollutants and promotes electron migration from the conduction band of the semiconductor to molecular oxygen [14]. Moreover, ammonium oxalate and CCl_4 respectively served as quenching agents for the hole (h^+) and electron, which proves that h^+ contributes to BPA degradation [26]. β-CD could capture h^+ generated by photogenerated charge separation and mediate the single-electron oxidation process of BPA [27].

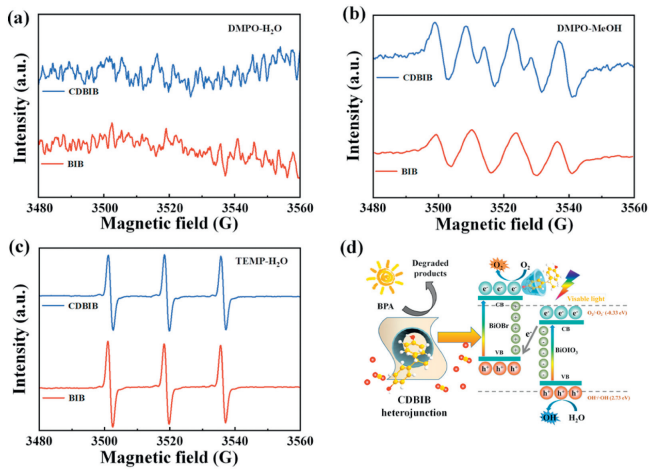

Fig. 9. (a) ESR spectra of DMPO-$^{\bullet}$OH, (b) ESR spectra of DMPO-$^{\bullet}O_2^-$, and (c) ESR spectra of TEMP-$^1O_2$. (d) Photocatalytic mechanism of BPA degradation over CDBIB under irradiation.

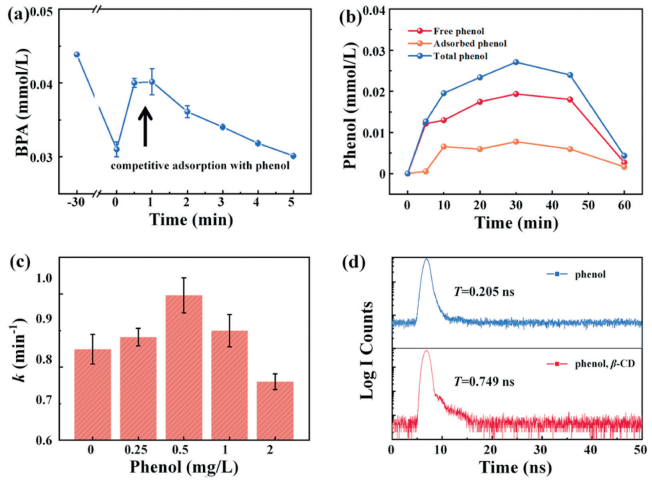

Fig. 10. (a) Removal efficiency of BPA by CDBIB (0–5 min). (b) Instantaneous concentration of phenol in BPA photooxidation by different catalysts, (c) effect of phenol on kinetics, and (d) time-resolved fluorescence spectra of phenol encapsulated by β-CD.

Electron spin resonance (ESR) was used to verify the ROS of CDBIB in the photocatalytic oxidation system. Fig. 9a does not show obvious quartet characteristic peaks of DMPO-$^{\bullet}$OH, which proves that ·OH was not the main ROS. The peak intensity of DMPO-$^{\bullet}O_2^-$ generated by CDBIB was greater than that of BIB (Fig. 9b). The peak intensity of TEMP-$^1O_2$ generated by CDBIB was weaker than that of BIB (Fig. 9c), implying the transformation of ROS and the increased generation of $^{\bullet}O_2^-$. On the basis of the free radical quenching experiment and EPR results, a plausible mechanism of the CDBIB heterojunction was proposed (Fig. 9d): The charge detachment mode between CD-BiOBr and $BiOIO_3$ conformed to the Z-scheme route [28]. The electrons transferred from the CB of $BiOIO_3$ to the VB of CD-BiOBr under light irradiation, and the electrons retained in the CB of CD-BiOBr acquired the ability to generate $^{\bullet}O_2^-$ [29]. Cyclodextrin loading remarkably promoted the dissolution and accumulation of photoelectrons in the Z-scheme charge disintegration of CDBIB [30].

We noted that the synergistic mechanism of β-CD for photocatalytic oxidation may proceed through avenues beyond simply enhancing the photocatalytic activity of the catalyst. The concentration of free BPA increased and then decreased at the initial stage of the reaction (Fig. 10a), which was considered to be the competitive adsorption site of the intermediate product phenol to replace part of the adsorbed BPA [31]. Phenol and BPA competed for adsorption and catalytic sites on the surface of CDBIB, but the degradation rate of BPA did not decrease. The concentration of free phenol continued to rise until BPA was completely degraded, which is contrary to the speculation that phenol and BPA compete for ROS (Fig. 10b). The adsorbed phenol was eluted with methanol to assess its concentration, and the concentration of adsorbed phenol was relatively constant (about 0.007 mmol/L) before BPA was completely degraded, indicating that the adsorbed phenol stably occupied a certain adsorption catalytic site (adsorbed BPA about 0.010 mmol/L). In accordance with the content of adsorbed phenol, we added phenol to the reaction system to investigate the change in the BPA degradation rate constant (Fig. 10c). A low concentration of phenol promoted the degradation of BPA, and the continuous addition of phenol hindered the degradation of BPA when the concentration of the added phenol was higher than 1 mg/L. Therefore, we speculate that the intermediate product (phenol) plays an autocatalytic role and does not hinder the degradation of BPA.

UV–vis spectroscopy was employed to monitor the inclusive behavior and thus understand the changes in the valence electron and the stability of organic radicals after the inclusion of BPA and phenol by β-CD (Fig. S2 in Supporting information). A hypochromic shift in BPA was observed with the increased addition of β-CD, which proves the possibility of $n\rightarrow n^*$ transition and the reduced reaction energy barrier [32]. The inclusion of phenol resulted in color enhancement, which may be due to the enhanced electron transfer through host–guest interactions. Similarly, the fluorescence intensity of BPA and phenol after β-CD inclusion was remarkably enhanced (Fig. S3 in Supporting information), which proves that β-CD stabilized its structure (Fig. S4 in Supporting information). The encapsulated bisphenol A was likely to be excited to the excited state, which is easily oxidized by $^{\bullet}O_2^-$ [33]. The fluorescence lifetime of phenol before and after β-CD inclusion was studied by time-resolved fluorescence spectroscopy (Fig. 10d), and the results showed that β-CD considerably prolonged the fluorescence lifetime of phenol [34]. Given that the primary photochemical process of phenolic pollutants is mainly a two-electron photoionization process, the enhancement of fluorescence lifetime prolongs the efficiency of two-electron ionization [35]. When ROS attack BPA to produce organic radicals (such as phenoxy radicals), β-CD stabilizes its structure and avoids self-coupling, thereby increasing the yield of free radicals [36]. When bisphenol A is completely degraded, the degradation rate of phenol increases because of the high reaction rate between phenoxy radicals and $^{\bullet}O_2^-$ [37].

3,3′,5,5′-Tetramethylbenzidine (TMB) was used as a substrate to investigate the radical yield in different systems and verify the conclusions above (Fig. 11a). The effects of phenol addition on the oxidation and discoloration of TMB in the BIB and CDBIB systems were investigated under simulated solar irradiation conditions (Figs. 11b and c) [38]. The results showed that the addition of phenol promoted the formation of free radicals in the CDBIB system, but phenol competed for free radicals in the BIB system. Through steric protection by host–guest chemistry, β-CD stabilized the phenoxy radicals formed by free radical oxidation, thereby inhibiting their dimerization [36]. However, UV radiation could not increase the photolysis efficiency of bisphenol A, which proves that the synergistic mechanism of cyclodextrin was not to improve the self-photolysis rate of the target pollutant. The free radical density in the β-CD supramolecular system could be increased by increasing the lifetime of phenoxy radicals. This conclusion is similar to that of a previous study, that is, cycloparaphenylene increases the yield of free radicals by stabilizing long-lived azafullerenyl radicals [39].

The excitation effect of β-CD on intermediate products was further verified. This work utilized Gaussian, Multiwfn [40] and Visual

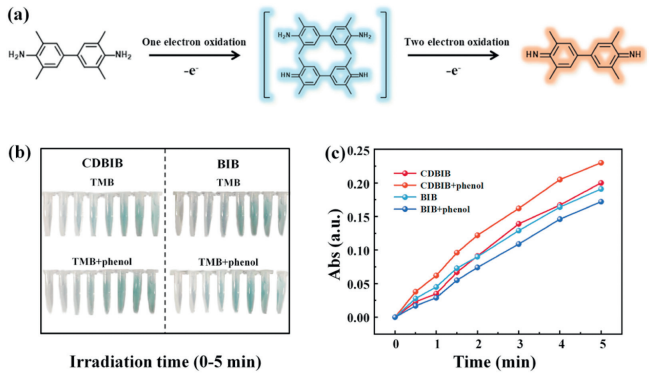

Fig. 11. (a) Mechanism diagram of TMB oxidation and color development, (b) photos of TMB with different catalysts, and (c) absorbance of TMB (700 nm, irradiated 0–5 min) with different catalysts.

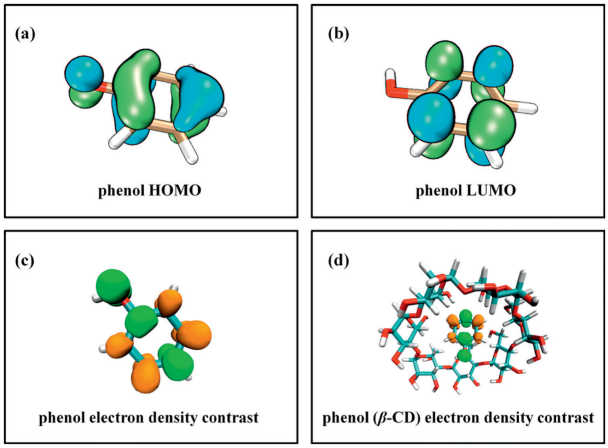

Fig. 12. Molecule configuration of phenol (a) HOMO and (b) LUMO. Equipotential surface diagram of electron excited state density contrast (c) phenol and (d) phenol encapsulated by β-CD.

Molecular Dynamics [41] software to analyze the charge characteristics of the main degradation intermediates in the CDBIB system [42]. The isopotential surface plot of the excited-state electron density difference shows that the inhomogeneity of the phenol charge encapsulated by β-CD increased in the excited state. The results of time-dependent density functional theory (TDDET) prove that the encapsulated phenol had high free radical reactivity, which easily produced a coupling reaction and increased the free radical yield [36].

Liquid chromatography–mass spectrometry was used to analyze the degradation intermediates and verify the effect of β-CD on the degradation pathway (Fig. S5 in Supporting information). The degradation pathway of BPA is shown in Fig. 12. The degradation mechanism of BPA could be divided into the following steps: C–C bond cleavage between quaternary carbon and the benzene ring, oxidative decarburization, hydroxylation caused by free radical attack of the BPA molecule, and coupled reaction (Fig. 13). In Route I, the C–C bond between quaternary carbon and the benzene ring was broken to produce phenol (**P2**) and *p*-methylphenol (**P2**) [17]. Subsequently, the phenolic hydroxyl group was continuously oxidized to form *p*-benzoquinone (**P17**), which easily opened the ring. In Route II, BPA was oxidized by ROS to form **P3**, which was gradually oxidized to form a carbonyl structure (**P11**) and further removed the hydroxyl group (**P15**) [43]. In Route III, the electrophilic ROS attacked the benzene ring to form a hydroxylated product (**P4**), which was further oxidized to form **P12** or converted into a quinone-containing intermediate (**P13**) [44]. These intermediates were oxidized to carboxylic acids (**P19**, **P20** and **P23**) by hydrogen extraction. In Route IV, **P1** and **P2** intermediates produced by the C–C bond cleavage of BPA coupled with BPA to form intermediates, such as **P5** and **P6**. The formed coupling products were easily attacked by ROS due to the quaternary carbon structure and further oxidized to **P14**, **P15** and **P16** [9]. Compared with the BIB system, the CDBIB system detected higher concentrations of phenol during the photocatalytic degradation of BPA and coupling oxidation product **P14** ($\tau = 8.8$ min). In addition, the particle flow intensities of the CDBIB system at retention times of 13.7, 14.05 and 14.9 min were much higher than those of the BIB system and corresponded to **P20**, **P6**, and *trans*-2,4-pentadienoic acid (*m/z* 112.98), respectively [45]. The loading of β-CD increased the content of intermediate phenol and the possibility of the coupling reaction by stabilizing the phenoxy radical. Moreover, the possibility of opening the ring through $^{\bullet}O_2^-$ increased, which is consistent with the previous conclusion.

The path of the photocatalytic oxidation of BPA in the CDBIB system was validated by calculating the electronic properties of BPA by using TDDFT (Fig. 14). The calculation results of the reduced Fukui function revealed that the hydroxyl ortho carbon atom of BPA had high free radical reaction activity and was easy to be attacked by free radicals to generate the hydroxyl addition reaction (**P4**) and the oxidative ring opening reaction (**P13**, Table S1 in Supporting information). The central quarterly carbon atom of the wrapped excited-state BPA had a high electron cloud density and was likely to be attacked by free radicals for exercise [43]. Phenol was the main product of the breaking of the quaternary carbon chain (Route III), which led to an increased concentration of phenol in the catalytic oxidation system of cyclodextrin.

After verifying the mechanism of β-CD synergistic degradation, we investigated the effect of water quality parameters on the photocatalytic degradation of BPA by the CDBIB system. Within a wide pH range, the CDBIB system exhibits excellent degradation effects on BPA, especially under alkaline conditions (Fig. S7 in Supporting information). In addition, coexisting substances in the water, such as anions and humic acids, have a minor impact on the photocatalytic oxidation of BPA by CDBIB (Fig. S8 in Supporting information). The cyclic stability and broad-spectrum performance of the CDBIB system have also been investigated. Fig. S9 (Supporting information) shows the reusability of the catalyst. Five cycles (1 h) were performed without cleaning for the next cycle. The degradation rate of phenolic pollutants by the CDBIB system was high, which is consistent with the abovementioned mechanism (Fig. S10 in Supporting information).

In this work, a β-CD-modified BiOBr@$BiOIO_3$ heterojunction photocatalyst was constructed to study the synergistic matrix of β-CD in photocatalytic oxidation reaction and clarify the non-catalyst-poisoning phenomenon caused by intermediate products of phenol. The photocatalytic performance of CDBIB was evaluated by BPA. The results showed that about 97% of BPA ($C_{[Cat.]} = 0.2$ mg/mL) was removed within 30 min, and the first-order kinetic constant ($k_{CDBIB} = 0.112$ min^{-1}) was about twice that of unloaded β-CD ($k_{BIB} = 0.057$ min^{-1}). CDBIB exhibits the accelerated electronic transmission ability and enhanced charge hole separation efficiency, and the stronger photoelectron reduction ability increases the yield of $^{\bullet}O_2^-$. In addition, the possible excitation effect of β-CD on the intermediate products was verified by spectroscopy and free radical chemistry. The synergistic mechanism of β-CD was mainly divided into the following points: (1) enhancement of photocatalytic performance and (2) excitation and stabilization of organic free radicals. CDBIB had a good anti-interference

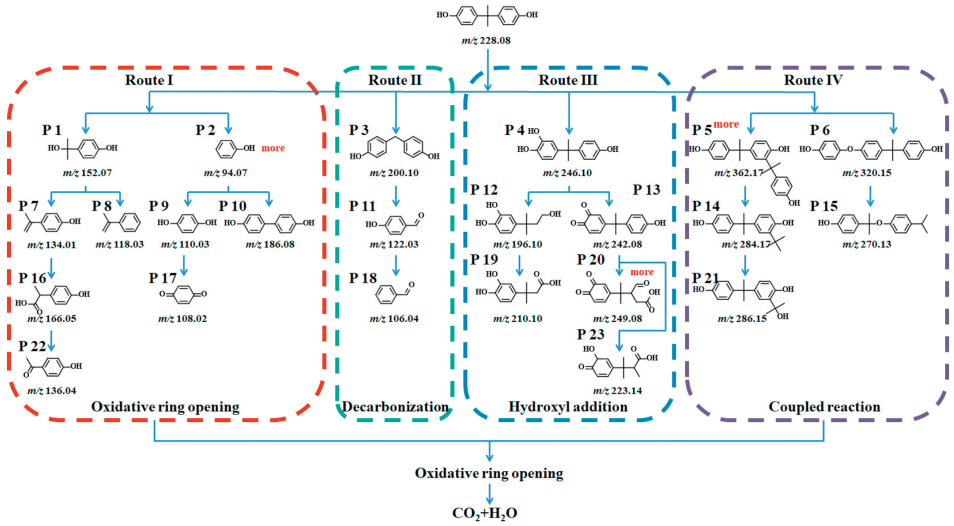

Fig. 13. Degradation pathway of BPA in the CDBIB photocatalytic oxidation system.

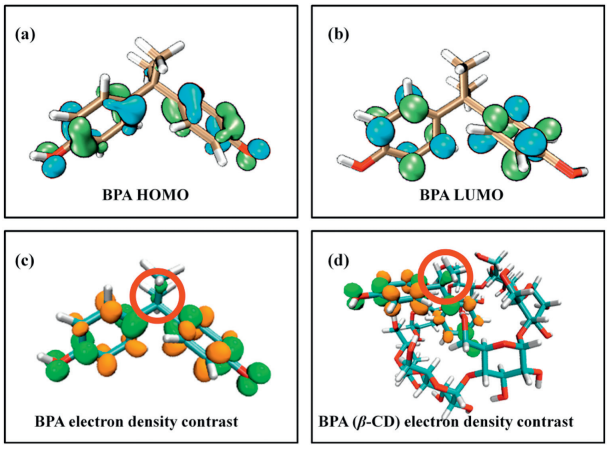

Fig. 14. Molecule configuration of BPA (a) HOMO and (b) LUMO. Equipotential surface diagram of electron excited-state density contrast (c) BPA and (d) BPA encapsulated by β-CD.

effect on the coexisting matrix of the water body and demonstrated certain cyclic stability.

Declaration of competing interest

The authors declare that they have no known competing financial interests or personal relationships that could have appeared to influence the work reported in this paper.

CRediT authorship contribution statement

Qinwei Lu: Conceptualization, Data curation, Methodology, Writing – original draft, Writing – review & editing. **Jinjie Lu:** Data curation, Writing – review & editing. **Juying Lei:** Writing – review & editing. **Xubiao Luo:** Supervision, Writing – review & editing. **Yanbo Zhou:** Conceptualization, Funding acquisition, Supervision, Writing – review & editing.

Acknowledgments

This work was supported by Program of Shanghai Outstanding Technology Leaders (No. 20XD1433900), the National Natural Science Foundation of China (No. 52370168).

Supplementary materials

Supplementary material associated with this article can be found, in the online version, at doi:10.1016/j.cclet.2024.110017.

References

[1] F. Dolan, J. Lamontagne, R. Link, et al., Nat. Commun. 12 (2021) 1915.
[2] C. Tortajada, P. van Rensburg, Nature 577 (2020) 26–28.
[3] S. Lim, J.L. Shi, U. von Gunten, D.L. McCurry, Water Res. 213 (2022) 118053.
[4] E. Stokstad, Science 375 (2022) 708.
[5] Y. Zhang, G. Huang, L. Winter, et al., Nat. Commun. 13 (2022) 3005.
[6] J. Jing, X. Wang, M. Zhou, Water Res. 232 (2023) 119682.
[7] Y. Zhou, J. He, J. Lu, Y. Liu, Y. Zhou, Chin. Chem. Lett. 31 (2020) 2623–2626.
[8] F. Chen, D. Tang, Y. Wang, J.H. Ma, Chemosphere 250 (2020) 126226.
[9] Y. Zhou, J. Lu, Q. Liu, et al., J. Hazard. Mater. 384 (2020) 121267.
[10] A.K. Das, S. Biswas, S.S. Manna, B. Pathak, S. Mandal, Chem. Sci. 13 (2022) 8355–8364.
[11] J. Wu, K. Xu, Q. Liu, et al., Appl. Catal. B 232 (2018) 135–145.
[12] Z. Miao, Q. Wang, Y. Zhang, L. Meng, X. Wang, Appl. Catal. B 301 (2022) 120802.
[13] Q. Liu, J. Wang, C. Duan, T. Wang, Y. Zhou, J. Hazard. Mater. 426 (2022) 128074.
[14] G. Sun, P. Tang, B. Ji, J. Hazard. Mater. 435 (2022) 128982.
[15] C. Duan, J. Wang, Q. Liu, Y. Zhou, Y. Zhou, Sep. Purif. Technol. 282 (2022) 120013.
[16] Y. Zhou, Q. Liu, J. Lu, et al., J. Hazard. Mater. 393 (2020) 122414.
[17] X. Chen, C. Duan, Y. Zhou, L. Yang, Y. Zhou, J. Clean. Prod. 395 (2023) 136323.
[18] X. Cai, Q. Liu, C. Xia, D. Shan, J. Du, J. Chen, Environ. Sci. Technol. 49 (2015) 9264–9272.
[19] Y. Yu, F. Chen, X. Jin, et al., Nanomaterials 13 (2023) 830.
[20] Q. Wang, Z. Yu, Q. Chen, et al., Sep. Purif. Technol. 300 (2022) 121781.
[21] E. Garcia-Diaz, D. Zhang, Y. Li, R. Verduzco, P.J.J. Alvarez, Water Res. 183 (2020) 116095.
[22] J. Lu, Y. Zhou, L. Ling, Y. Zhou, Chem. Eng. J. 446 (2022) 137067.
[23] Y. Qing, Y. Li, L. Cao, et al., Sep. Purif. Technol. 314 (2023) 123545.
[24] Q. Gao, B. Weng, P. Jin, A. Volodine, L. Sun, B. Van der Bruggen, et al., Chem. Eng. J. 446 (2022) 137316.
[25] T.A. Oproglidis, D.H. Tassis, A. Tsormpatzoglou, et al., Solid State Electron. 197 (2022) 108451.
[26] Z. Chen, H. Guo, H. Liu, et al., Chem. Eng. J. 438 (2022) 135471.
[27] C. Chen, Y. Kuo, Y. Lin, et al., ACS Appl. Mater. Interfaces 14 (2022) 9587–9596.
[28] Y. Gong, X. Quan, H. Yu, S. Chen, H. Zhao, Appl. Catal. B 237 (2018) 947–956.
[29] L. Meng, C. Zhao, T. Wang, H. Chu, C. Wang, Sep. Purif. Technol. 313 (2023) 123511.
[30] J. Shi, Y. Chen, Q. Wang, Y. Liu, Adv. Mater. 22 (2010) 2575–2578.
[31] Y. Zhou, Q. Liu, X. Li, L. Ling, Y. Zhou, Chem. Asian J. 17 (2022) e202200352.
[32] Q. Hao, Y. Kang, J.F. Xu, X. Zhang, Langmuir 37 (2021) 6062–6068.
[33] H. Wang, K. Xue, Y. Yang, et al., J. Am. Chem. Soc. 144 (2022) 2360–2367.
[34] G. Wang, W. Fan, Q. Li, N. Deng, Chemosphere 216 (2019) 707–714.
[35] S. Zhang, H. Lan, Y. Cui, X. An, H. Liu, J. Qu, Environ. Sci. Technol. 56 (2022) 3552–3563.
[36] B. Tang, J. Zhao, J.F. Xu, X. Zhang, Chem. Sci. 11 (2020) 1192–1204.
[37] J. Deng, C. Zhou, Y. Yang, et al., Chem. Eng. J. 462 (2023) 142282.
[38] L. Zhang, Q. Tan, S. Xiao, et al., Small 19 (2023) 2207798.

[39] A. Stergiou, J. Rio, J.H. Griwatz, et al., Angew. Chem. Int. Ed. 58 (2019) 17745–17750.
[40] T. Lu, F. Chen, J. Comput. Chem. 33 (2012) 580–592.
[41] W. Humphrey, A. Dalke, K. Schulten, J. Mol. Graph. 14 (1996) 33–38.
[42] Z. Xie, C. He, H. Zhou, et al., Environ. Sci. Technol. 56 (2022) 8784–8795.
[43] Z. Zhang, J. Liu, P.Y. Gu, et al., Sep. Purif. Technol. 287 (2022) 120539.
[44] F. Chang, S. Zhao, Y. Lei, et al., Sep. Purif. Technol. 304 (2023) 122324.
[45] J. Shen, A. Shi, J. Lu, et al., Environ. Pollut. 323 (2023) 121186.